Journal of Membrane Science 459 (2014) 177–189

Contents lists available at ScienceDirect

Journal of Membrane Science

journal homepage: www.elsevier.com/locate/memsci

Probing membrane and interface properties in concentrated electrolyte solutions

Enrica Fontananova [a,*], Wenjuan Zhang [a], Isabella Nicotera [b], Cataldo Simari [b], Willem van Baak [c], Gianluca Di Profio [a], Efrem Curcio [d], Enrico Drioli [a,d]

[a] Institute on Membrane Technology of the National Research Council (ITM-CNR), c/o University of Calabria Via P. Bucci, cubo 17/C, 87036 Rende (CS), Italy
[b] Department of Chemistry and Chemical Technologies, Via P. Bucci, University of Calabria, 87036 Rende (CS), Italy
[c] Fujifilm Manufacturing Europe BV, Tilburg, The Netherlands
[d] Department of Environmental Engineering and Land and Chemical Engineering, University of Calabria Via P. Bucci, cubo 44A, 87036 Rende (CS), Italy

ARTICLE INFO

Article history:
Received 23 August 2013
Received in revised form
24 January 2014
Accepted 25 January 2014
Available online 17 February 2014

Keywords:
Concentrated electrolyte solution
Impedance
Interface
Ion exchange membrane
PGSE-NMR

ABSTRACT

This study deals with the membrane and interface electrical properties investigation by electrochemical impedance spectroscopy (EIS). The EIS is a powerful technique for characterizing electrical behavior of systems in which coupled electrical processes occur at different rates. A systematic study on the effect of solution concentration, temperature and velocity, on the electrical resistance of anion- and cation-exchange membranes (AEMs and CEMs) and their interfaces (electrical double layer and diffusion boundary layer), was carried out. At the best of our knowledge, for the first time electrolyte concentrations up to 4 M were used for the study of membranes and interface by EIS.

Moreover, Pulsed Gradient Spin Echo Nuclear Magnetic Resonance (PGSE-NMR) technique was used to measure the water self-diffusion coefficients in swelled membrane as a function of the solution concentration and temperature. These measurements gave additional important insights about the effect of the electrolyte solution and fixed charges concentration in membrane, on membrane microstructure and its transport and electrical properties.

1. Introduction

One of the major concerns of membranologists operating in the field of electro-membranes processes, is the depth knowledge of the membrane electrical and mass-transport properties. It is known that at the interface between a solid ionic conductor and a liquid electrolyte, physical and electrical properties change suddenly because of an heterogeneous charges distribution (polarization) which reduce the overall electrical conductivity of the system [1–3].

The membrane electrical resistance is usually measured by direct current (DC) method. In DC measurements the membrane is installed in a cell which consists of two chambers containing the testing solutions separated by the membrane. A DC signal is applied and the voltage drop across the membrane is measured. The electrical resistance is given by the slope of the current vs. the voltage drop curve, in agreement with Ohm's law [4]:

$$R = \frac{U}{I} \tag{1}$$

where R [Ω] is the resistance, U [V] is the voltage drop measured between the two sides of the membrane; I [A] is the current.

To obtain the membrane resistance, the resistance of the cell filled with the solution, but without the membrane, is subtracted from the resistance of the cell containing both, the solution and the membrane. The method is simple, but it is not able to distinguish the membrane from the interface resistance. On the contrary of the measurement in direct current, using an alternate current (AC) over a frequency range, it is possible to distinguish phenomena proceeding at different rates. Electrochemical Impedance Spectroscopy (EIS) is a powerful technique in which an AC is used to measure quantitatively the resistance to the charge transport in the bulk and interfacial regions of solid and liquid electrolyte materials [1,5–7].

In EIS experiments a sinusoidal electrical stimulus (voltage or current) is applied over a frequency range to a pair of electrodes and the response of the system under investigation is observed (current or voltage) by the same, or different electrodes. In the first case the configuration is indicated as two probes (or two electrodes) configuration; when two additional electrodes are used to collect the response of the system, the configuration is indicated as a four probes [1]. In membrane characterization field, the two probe configuration is usually applied when the membrane is pressed

* Corresponding author. Tel.: +39 098 449 2010; fax: +39 098 440 2103.
E-mail addresses: e.fontananova@itm.cnr.it, enrica.fontananova@cnr.it (E. Fontananova).

http://dx.doi.org/10.1016/j.memsci.2014.01.057
0376-7388

between two solid conductive electrodes, like in the case of the membrane electrode assembly (MEA) for fuel cells [8–11].

Despite some examples of the use of the two probes configuration can be found in literature for the study of the ion transport through a membrane separating two liquid electrolyte solutions [12–14], the four probe configuration is the most convenient and commonly used. The four probes, with respect to the two probes configuration, has the advantage to eliminate from the impedance spectra the contribution of the electrode injecting stimulus/electrolyte charge transfer resistance, focusing the probing on the membrane and its interface [15–21]. Impedance spectroscopy was also used for the in-situ non-destructive structural characterization of membranes and fouling phenomena [17,22–24]

Another possible configuration in EIS experiments consist in the use of three electrodes, but it is usually employed to characterize only one half of an electrolytic/electrochemical cell, or phenomena occurring on an electrode [25], but not to investigate membrane properties.

This study deals with the membranes and interface electrical properties investigation by EIS. A systematic analyses on the effect of solution concentration, temperature and velocity on the electrical resistance of anion and cation exchange membranes (CEMs and AEMs) and their interfaces, was carried out. At the best of our knowledge, for the first time electrolyte concentrations up to 4 M were used for the study of membranes and interface properties by EIS. Moreover, Pulsed Gradient Spin Echo Nuclear Magnetic Resonance (PGSE-NMR) technique was used to characterize AEMs and CEMs swelled in concentrated electrolyte solutions. NMR spectroscopy provides information on the microscopic, as well as, macroscopic nuclear environments by determination of parameters such as relaxation times, self-diffusion coefficients, and structural information.

The interest towards concentrated solutions lies in the high salinity-gradient power (SGP) that can be extracted by membrane-based energy conversion processes, like pressure-retarded osmosis (PRO) and reverse electrodialysis (RE). The maximum theoretical obtainable energy during the reversible mixed of a diluted stream with a saline concentrated solution, ranges from 0.75 kW-h/m^3 to 14.1 kW-h/m^3 of diluted solution, going from seawater (osmotic pressure 2.7 MPa) to Dead Sea water (osmotic pressure 50.7 MPa) as saline solution [26]. Concentrated solutions are produced in numerous industrial activities such as saltworks and salt mines. Membrane-based integrated systems open interesting perspectives for sustainable and efficient energy conversion using natural and abundant water resources. Brine solutions can be produced by reverse osmosis and/or membrane distillation of seawater [27–30], and they can be used as concentrated stream in SGP-RE stack employing as diluted stream sea or brackish water. This idea is at the basis of the European FP7 Project Reapower (www.reapower.eu), and it can offer a huge potential for the improvement of the electrical performance of SGP-RE system, which usually focus on the combination of fresh water, as the diluted solution, and seawater, as the concentrated solution. The use of concentrated solution allows to reduce the electrical resistance within the low concentration compartment of the SGP-RE stack, boosting the power that can be extracted from the SGP [26,31,32].

2. Materials and methods

2.1. Membranes samples

Three homogeneous reinforced cation exchange membranes (CEMs) and three homogenous reinforced anion exchange membranes (AEMs) produced by Fuji, were investigated (Table 1). Before the use the membranes were washed with a 0.5 M NaCl solution for 24 h changing the solution 4 times to remove residual traced of solvents and/or chemical agents. After this procedure the samples were indicated as “activated”.

2.2. Electrohemical impedance spectroscopy (EIS) experiments

In EIS experiments the response of a system to a sinewave voltage or current excitation is investigated in the frequency domain. Voltage ($U_{(\omega)}$ [V]) and current ($I_{(\omega)}$ [A]) depend from the circular velocity or circular frequency ω [s^{-1}] as follow:

$$U_{(\omega)} = U_o \sin \omega t \tag{2}$$

$$I_{(\omega)} = I_o \sin(\omega t + \varphi) \tag{3}$$

$$\omega = 2\pi\nu \tag{4}$$

where t [s] is the time, φ [°] is the phase shift between voltage and current, and the subscript o refers to the amplitude of voltage and current in phase, ν [s^{-1}] is the frequency.

By using the Euler form:

$$e^{j\varphi} = \cos \varphi + j \sin \varphi \tag{5}$$

where j is the imaginary number ($j = \sqrt{-1}$)

The impedance $Z_{(\omega)}$ [Ω] can be expressed in a form similar to Ohm's law:

$$Z_{(\omega)} = \frac{U_o e^{j\omega t}}{I_o e^{j(\omega t+\varphi)}} = \frac{U_o}{I_o} e^{j\varphi} = |Z| \cos \varphi + j|Z| \sin \varphi \tag{6}$$

where $|Z|$ is the impedance modulus.

The Eq. (6) indicates that the impedance is composed of two parts, i.e. the real part:

$$Z' = |Z| \cos \varphi \tag{7}$$

and the imaginary part:

$$Z'' = |Z| \sin \varphi \tag{8}$$

The real part of the impedance is the resistance, the imaginary part is called reactance [1,4].

Table 1
List and some experimentally determined properties of the membranes.

Membrane	Thickness (μm)*	Ion exchange capacity (mmol/g membrane)	Density of fixed charges (mol/L)*	Membrane areal resistance (Ω cm^2)**
Fuji-AEM-0150	166 ± 1	1.1 ± 0.1	2.2 ± 0.3	1.631 ± 0.001
Fuji-AEM-80045	129 ± 2	1.4 ± 0.1	3.8 ± 0.2	1.551 ± 0.001
Fuji-AEM-90025	109 ± 2	1.6 ± 0.3	2.9 ± 0.6	1.102 ± 0.001
Fuji-CEM-0150	170 ± 1	1.6 ± 0.1	3.4 ± 0.2	2.647 ± 0.001
Fuji-CEM-80050	114 ± 2	1.1 ± 0.1	2.4 ± 0.2	2.974 ± 0.001
Fuji-CEM-90026	113 ± 2	1.0 ± 0.3	1.8 ± 0.5	1.642 ± 0.001

* Conditions: NaCl 0.5 M, 20 °C.
** Conditions: NaCl 0.5 M, 20 °C, 2.8 cm s^{-1}.

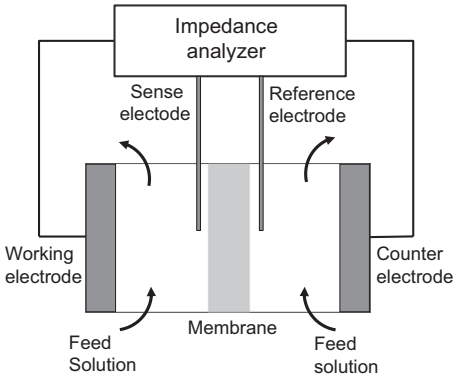

Fig. 1. Schematic view of the experimental set-up used for the EIS experiments.

In this work a four electrodes configuration was used with a home designed impedance cell having an active membrane area of 3.14 cm^2 (Fig. 1). The membrane disc was placed in vertical position.

The cell was fed by two gear pumps with two identical solutions (1 L for each solution), immersed in a thermostatic bath and kept under stirring, flowing along the opposite sides of the membrane. An AC current over a frequency range was injected through two planar electrodes (working and counter electrode) and the response of the system to the sinewave perturbation was measured by two reference electrodes (indicated as sense and reference) using a potentiostat/galvanostat combined with a frequency response analyzer, Metrohm Autolab Autolab PGSTAT302N. The voltage drop across the membrane was measured by positioning the two reference electrodes in symmetric Haber–Luggin capillaries having the tip close to the membrane surface. The cell was inserted inside a thermostatic Faraday cage connected to the potentiostat/galvanostat ground for proper shielding.

The sense and reference electrodes were Ag/AgCl Reference electrodes from Gamry Instruments; the Haber–Luggin capillaries were filled with KCl 3 M. The planar working and counter electrodes were made of Ag covered with a thin layer of AgCl by electro deposition. Milli-Q water (18.2 MΩ cm) was used to prepare all the solutions.

The EIS experiments were carried out in the frequency range 1000–0.01 Hz, with a signal amplitude of 10 mV. The electrical resistance [Ω] was multiplied for the active area [cm^2] to obtain the areal resistance [Ωcm^2].

Each sample, after activation, was immersed in the testing solution for 24 h to ensure a complete conditioning. The EIS spectra were fitted with the equivalent circuits [1,12] showed in Fig. 2, by the software Nova 1.9.16 by Metrohm Autolab B.V., using a non-linear least square procedure (convergence conditions: maximum number of iterations 1000; maximum number of iterations without improvement 50; maximum change in χ^2 (scaled) parameter 0.001). If not otherwise specified, the circuit A, was used. The membrane resistance (R_m) was obtained subtracting the solution resistance, obtained from blank experiments (i.e. without the membrane), from the membrane plus solution resistance (R_{m+s}). All the experiments have been repeated in triplicate.

2.3. Ion exchange capacity

The ion exchange capacity (IEC) was measured by acid–base titration. A sample of activated CEM or AEM was thoroughly washed with water to remove residual traces of salt on the surface and immersed respectively in a known volume of 0.1 M solution of HCl or NaOH for three days at 20 ± 2 °C. Then the membrane was removed and the exchanged solution was divided in three lots that were titrated respectively with 1 M NaOH or HCl solution until neutrality (pHmeter immersed in the solution).

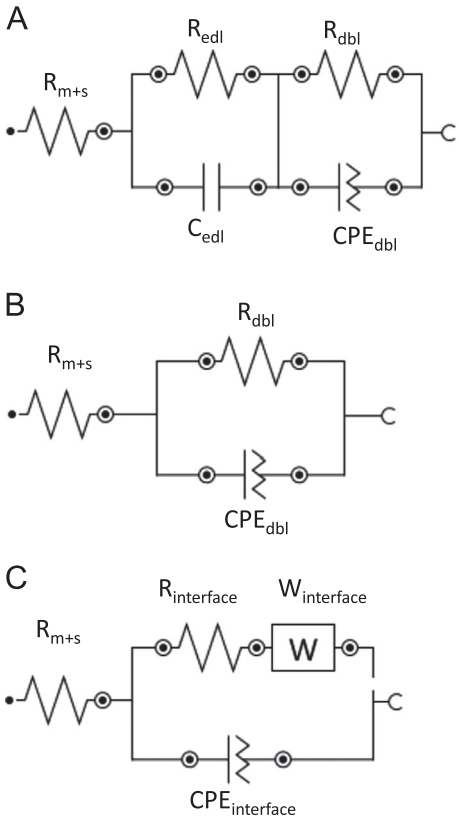

Fig. 2. Equivalent circuits used to fit the EIS spectra. The resistor is indicated as *R*; the capacitor as *C*; the constant phase element (a non-ideal capacitor) as CPE; the Warburg impedance as *W*. The subscript "*m+s*" is referring to membrane plus solution, the subscript "edl" to the electrical double layer; the subscript "dbl" to the diffusion boundary layer; the subscript "interface" indicates the global interface membrane/solution.

The IEC was calculated using the following equation:

$$IEC = \frac{\text{moles } H^+ \text{ or } OH^- \text{ exchanged}}{W_{dry}} \quad (9)$$

The dry weight of the membrane (W_{dry} [g]) was measured after the exchange, by washing the membrane thoroughly with water and drying the sample in a furnace at 80 °C for 2 days.

The procedure was repeated three times and the medium value was reported.

2.4. Membrane swelling

The membrane swelling was determined by immersing the activated samples in a NaCl solution (0.017 M; 0.5 M; 1 M or 4 M) for three days at a fixed temperature (20 °C; 30 °C or 40 °C). In the case of the swelling experiments with the 0.017 M NaCl solution, the activation procedure was carried out using this diluted solution instead of the 0.5 M solution.

The wet weight (W_{wet} [g]) was measured after swelling in the salt solution and rapid dipping of the membranes on the surface with paper tissue. The dry weight (W_{dry} [g]) was measured after the exchange procedure, as reported above.

The membrane swelling (*sw%*) was calculated using the following formula:

$$sw\% = \frac{W_{wet} - W_{dry}}{W_{dry}} 100 \quad (10)$$

The swelling and the IEC data were used to determine the density of the fixed charged groups (moles of fixed charged groups per volume of water in membrane, C_{fix} [mol/L]) at various

temperatures (20–40 °C) and solution concentrations (0.017–4 M):

$$C_{fix} = \frac{IEC}{sw\%}100 \quad (11)$$

2.5. PGSE-NMR analyses

NMR measurements were performed on a Bruker NMR spectrometer AVANCE 300 Wide Bore working at 300 MHz on ^{1}H. The employed probe was a Diff30 Z-diffusion 30 G/cm/A multinuclear with substitutable RF inserts. Spectra were obtained by applying the Fourier transform to the resulting free induction decay (FID) of a single $\pi/2$ pulse sequence. The $\pi/2$ pulse width was about 8 μs. One of its most important uses in the study of swelled membranes has been to provide mass transport data of the diffusing ions through measurement of water self-diffusion coefficient (D) by the NMR pulse gradient spin echo (PGSE) sequence [33] (Fig. 3A). The PGSE technique is a powerful non-invasive method for the determination of D in multi-component systems and consists of two rf pulses, Hahn-echo sequence ($\pi/2$–τ–π), with two identical pulsed-field gradients, the first applied between the 90° and 180° rf pulse (during the dephasing) and the second after the 180° rf pulse (during the rephasing) but before the echo. Following the usual NMR notation, the pulsed-field gradients have magnitude g, duration δ, and time delay Δ (different from the degree of ionic association). The attenuation of the echo amplitude is represented by the Stejskal–Tanner equation:

$$A(g) = A(0)e^{-\gamma^2 g^2 D\delta^2(\Delta-\delta/3)} \quad (12)$$

where D is the self-diffusion coefficient and γ is the nuclear gyromagnetic ratio and $A(0)$ is the amplitude of the echo at $g=0$. Note that the exponent in the equation is proportional to the mean-squared displacement of the molecules over an effective time scale ($\Delta-(\delta/3)$). For the investigated samples, the experimental parameters, Δ and δ, were 10 and 1 ms, respectively. The gradient amplitude, g, varied from 10 to 600 G cm^{-1}. In this conditions the uncertainty in the self-diffusion measurements was ~3%.

Finally, longitudinal relaxation times (T_1) were measured by the inversion-recovery sequence (π–τ–$\pi/2$) (Fig. 3B).

The time interval τ was varied using approximately 10–12 values. Immediately following the π pulse, the magnetization (M) was inverted. During the time interval, M relaxed back to thermal equilibrium at a rate of T_1^{-1}. The application of the $\pi/2$ rf pulse caused M to rotate from the z-axis into the x–y plane where the nuclear signal may be picked up by a receiver. The time dependence of Mz follows:

$$Mz = Mo(1-2e^{-\tau/T1}) \quad (13)$$

For the NMR measurements, two membrane samples were selected: Fuji-AEM-80045 and Fuji-CEM-80050. Each activated membrane was conditioned in the testing solution for 24 h, then it was removed from the solution and quickly blotted dry on the surface with a paper tissue. At this point the membrane was loaded into a 5 mm NMR Pyrex tube and put in the spectrometer. The measurements were conducted by increasing temperature step by step from 20 to 100 °C, and leaving the sample to equilibrate at each temperature for about 10 min.

3. Results and discussion

3.1. Effect of the solution velocity and temperature on the membrane and interface resistances

The membranes were characterized by EIS using a 0.5 M NaCl solution, simulating the seawater. The EIS spectra were fitted with

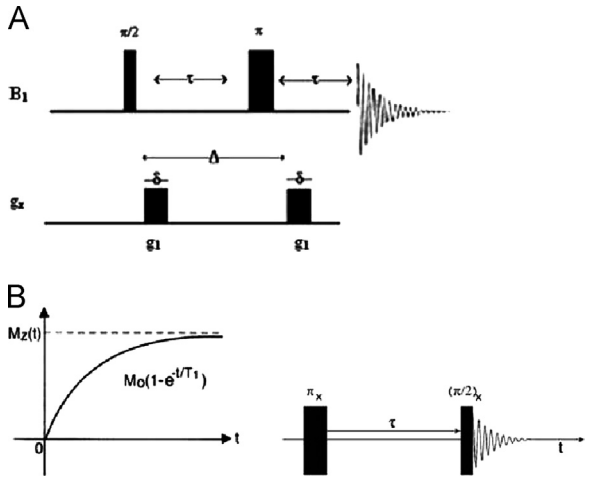

Fig. 3. Schematic of the pulse gradient spin echo technique (PGSE) pulse sequence (A); inversion recovery sequence (B).

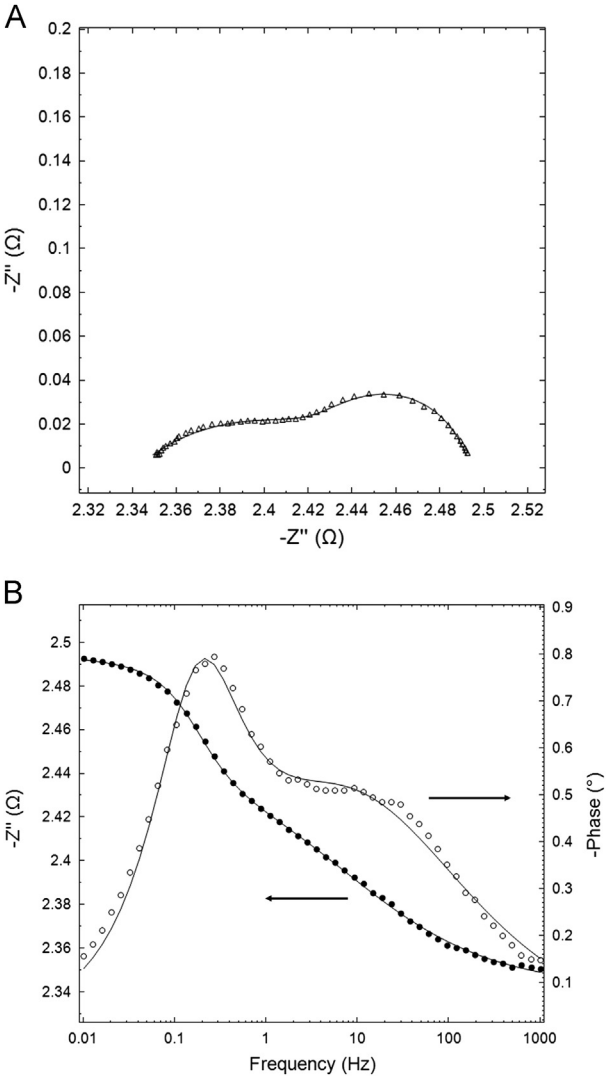

Fig. 4. Nyquist (A) and Bode plot (B) of the Fuji-CEM-0150 membrane measured in 0.5 M NaCl solution at 20 ± 1 °C and 2.8 cm s^{-1}. In (A): $Z'(\Omega)$ is the real part and $-Z''(\Omega)$ is the imaginary part of the impedance; in (B): $Z(\Omega)$ is the module of the impedance and Phase (°) is the phase shift between voltage and current. The experimental data (symbols) were fitted with the equivalent circuit of Fig. 2A (continuous line).

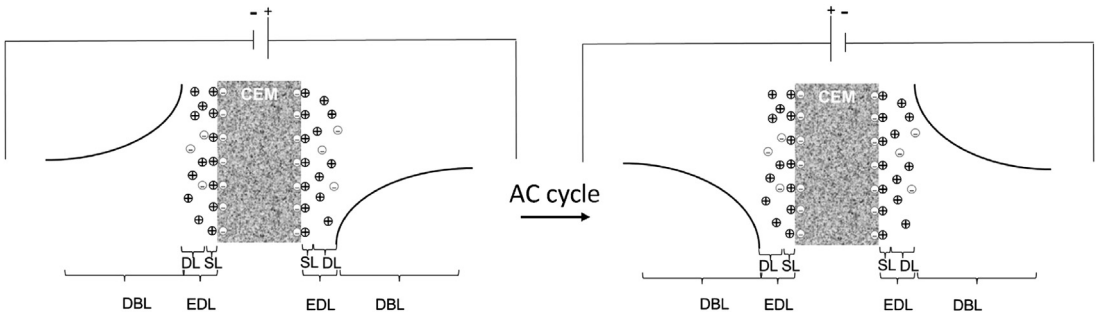

Fig. 5. Bipolar concentration polarization for a cation exchange membrane (CEM) immersed in an electrolyte solution during an AC cycle. Schematic view of the diffusion boundary layer (DBL) and the electrical double layer (EDL), composed by the Stern layer (SL) and the diffusion layer (DL). The continuous line in the DBL is the qualitative salt concentration profile.

the equivalent circuit of Fig. 2A. The Nyquist plot (Fig. 4A), which shows the imaginary part vs. the real part of the impedance, and the Bode plot (Fig. 4B), which represents the module of the impedance and the phase shift dependence vs. the frequency, provides a visual verification of the good agreement between the equivalent circuit proposed and the experimental data.

The circuit of Fig. 2A includes, in addition to the membrane and solution resistance (R_{m+s}) the contribution of the interfacial transfer resistance through the electrical double layer (R_{edl}) and the diffusion boundary layer (R_{dbl}). The formation of the electrical double layer is due to the presence of a net charge on the membrane surface which affects the ions distribution at the membrane/solution interface, resulting in an increase in the concentration of counter-ions (Fig. 5). The region over which this influence spreads out is called electrical double layer (EDL) [3,34,35]. The EDL is schematically composed by two layers: an inner layer, called *Stern layer* (SL), formed by ions strongly bound by electrostatic interactions with the membrane surface, and an outer layer, called *diffuse layer* (DL), constituted by loosely bond ions. The SL has a thickness in the order of Angstrom (one or two radius of solvated ions away from the surface); the DL has a thickness in the order of nanometer. The counter ions in the DL are less attracted to the charged surface because of the electrically screening of the SL, and they tend to diffuse into the liquid phase under the influence of electrical attraction and thermal motion. Fig. 5.

Moreover, concentration polarization phenomena occurs at the interface membrane/solution because of the flux difference between the co-ion and the counter-ion, as well as, because of the difference in transport number of the ions between the ion-exchange membrane (IEM) and the solution phase [36,37].

In a IEM the electrical current is transported almost exclusively by the counter-ions having a transport number in membrane tending to one. On the contrary, the co-ions are ideally excluded within the IEM due to the presence of fixed ions of the same sign (Donnan exclusion), and the transport number tends to zero. In the solution phase the current is transported both by co- and counter-ions and, in the case of symmetric salts, the transport number is 0.5 for both. As a consequence an additional layer, called diffusion boundary layer (DBL), having a thickness in the order of several hundred of micrometers, is formed (Fig. 5).

The membrane resistance did not change significantly with the solution velocity (Fig. 6). This behavior can be also easily appreciated comparing the Nyquist plot registered at different velocities (Fig. 7). The intercept with the real axis of the impedance at high frequency corresponds to the membrane plus solution resistance (R_{m+s}) and it was substantially independent from the solution velocity. On the contrary, the intercept at low frequency, which contains also the contribution of the interface ($R_{m+s}+R_{edl}+R_{dbl}$), was visibly reduced increasing the solution velocity. In particular, the resistance of the diffusion boundary layer decreased for all the samples with increasing solution velocity.

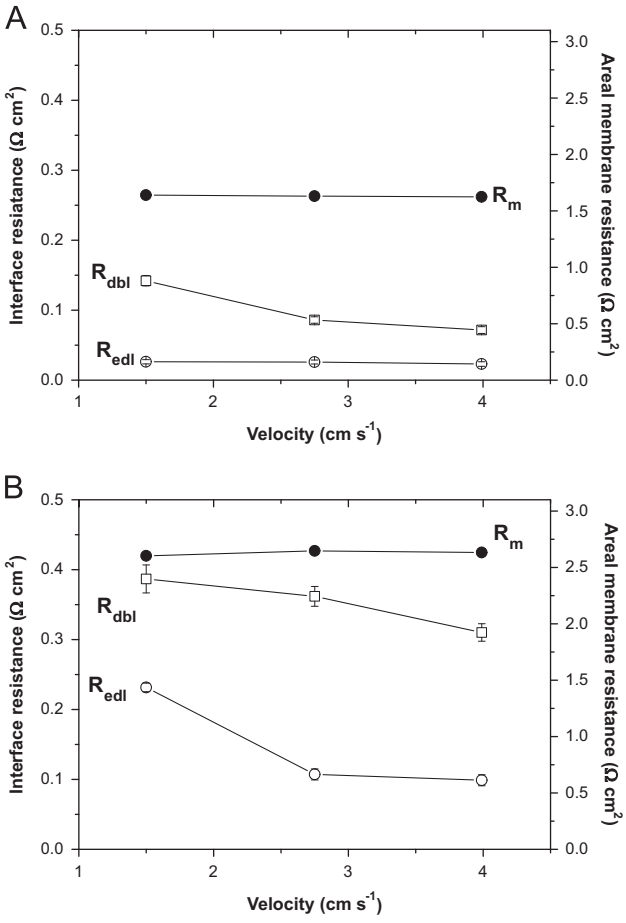

Fig. 6. Membrane (R_m) and interface (R_{edl} and R_{dbl}) areal resistances as a function of the solution velocity of the Fuji-AEM-0150 (A) and the Fuji-CEM-0150 (B). Conditions: 0.5 M NaCl, 20 ± 1 °C. Filled symbols, axes on the right for the R_m; empty symbols, axes on the left for the R_{edl} and R_{dbl}.

The bipolar concentration polarization during AC cycle caused by the buildup and depletion of ions at the interface, was time dependent. The contribution of the interfacial ionic charge transfer through the interface layers at low frequencies was greater than at high frequencies, because at high frequencies there is insufficient time for their formation.

The resistance of the membrane was the dominant resistance with respect the interfacial ionic charge transfer through the electrical double layer and the diffusion boundary layer ($R_m > R_{dbl} > R_{edl}$).

The velocity did not influence significantly R_{edl} in the case of the AEMs, but it had a not negligible effect in the case of CEMs.

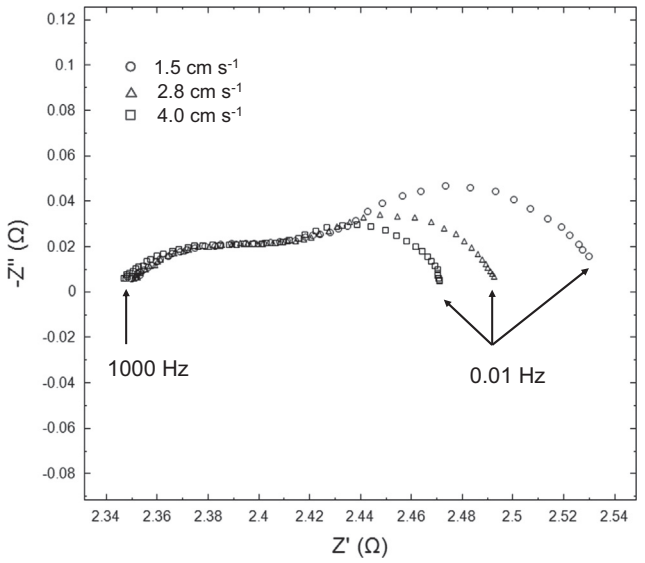

Fig. 7. Nyquist plot of the Fuji-CEM-0150 membrane measured in a 0.5 M NaCl solution at 20 ± 1 °C at different velocities: 1.5 (symbol: circle), 2.8 (symbol: triangle) and 4.0 cm s^{-1} (symbol: square).

This was probably due to a higher thickness of the DL in the EDL, with respect to the AEMs, which renders the influence of the tangential stress more relevant. The higher thickness of EDL of the CEM is related to the greater hydrodynamic radius of the counter-ion in the case of the CEMs with respect to the AEMs (respectively Na^+ and Cl^-).

The membrane and interface resistances of the CEMs, were higher in comparison with the AEMs resistances (Table 1). The higher resistances observed with the CEMs with respect to the AEMs were dependent from the lower mobility of the Na^+ ion with respect to the Cl^- (4.98×10^{-8} and 6.88×10^{-8} m^2 V^{-1} s^{-1} respectively at 25 °C [38]). This increased not only the membrane electrical resistance, but also the interface resistances where the counter-ions concentration was higher than co-ions.

The membrane areal resistance of the AEMs with 0.5 M NaCl decreased in the order: Fuji-AEM-0150 > Fuji-AEM-80045 > Fuji-AEM-90025. These results were in agreement with the decreasing thickness of the membranes in the same order (Table 1). This means that the reduction of the membrane thickness can contribute to reduce the electrical resistance. However, also the fixed charge density, the chemical nature and distribution of the fixed charged groups, are key factors for the membrane electrical resistance. In general, increasing the density of the fixed charged groups the ions migration through the membrane is expected to be more limited because of the stronger interactions of the mobile ions with the fixed ions [39]. For this reason, despite the Fuji-CEM-80050 and Fuji CEM-90026 had similar thickness, the electrical resistance of the second one was lower thanks to its lower density of the fixed charged groups

The resistance of the ion transport through the membrane, as well as through the interface, decreased with the temperature, because of the increasing ion mobility (Fig. 8). The effect of the temperature was more evident for the CEMs than for the AEMs.

3.2. *Effect of the solution concentration on the membrane and interface resistances*

In addition to the temperature and the solution velocity, another important factor able to influence the electrical resistance of the IEMs, was the solution concentration. Increasing the concentration from 0.5 M to 1 M resulted in a drop of the membrane and the interfacial ionic charge transfer resistances for the Fuji-AEM-90025 and the Fuji-CEM-90026 (Table 2).

In the case of the Fuji-AEM-80045 and Fuji-CEM-80050 membranes, the EIS experiments were conducted also with a 4 M NaCl solution. This solution simulates the seawater brine. With the 4 M solution the fitting with the model represented in the Fig. 2A did not converge for most of the experiments. Only in few cases, the model converged but it gave a R_{edl} values very low (in the order of few μΩ) or negative (without physical meaning), and the estimated error was very high (> 100%). On the contrary the experimental data were fitted reaching a good convergence with the equivalent circuit represented in Fig. 2B. As a consequence, it was possible to draw the conclusion that the contribution of the electrical double layer to the total resistance became negligible at 4 M NaCl. This behavior was in agreement with the reduction of the thickness of the electrical double layer increasing the solution concentration, because of the higher screening effect of the attractive electrical interactions between the counter-ions and fixed charged groups of the membrane, increasing the ions concentration in solution [40]. The thickness of the electrical double layer is approximately the Debye length, which is reciprocally proportional to the square root of the ionic strength of the solution, or ionic concentration in the case of symmetric electrolytes [41].

Also in the case of the 4 M solution, like for the 0.5 M solution, the ion transport resistance decreased with the increasing of the temperature (Fig. 8C and D).

Increasing the solution concentration from 0.5 M NaCl to 4 M, the membrane resistance decreased slightly for the Fuji-AEM-80045, and the resistance of the diffusion boundary layer increased (Table 2).

An opposite behavior was observed for the Fuji-CEM-80050: increasing the solution concentration the membrane resistance increased but the resistance of the diffusion boundary layer decreased (Table 2).

However, considering also the decreasing of the solution resistance, increasing the concentration up to 4 M, the effect on the total cell resistance ($R_{m+s}+R_{dbl}+R_{edl}$) was a net reduction. For example for the Fuji CEM-80050 at 20 ± 1 °C and 1.5 cm s^{-1} the total resistance decreased from 8.0 to 4.5 Ωcm^2, increasing the solution concentration from 0.5 to 4 M.

The increase of the membrane electrical resistance, was due to the membrane shrinking induced by the increasing solution concentration (Fig. 9A), with a consequent narrowing of the hydrophilic channels of the IEMs (pathway for the ions transport) [42]. In parallel, the fixed charge density increased with the reduction of the swelling degree and, as a consequence, the ion migration through the membrane was more difficult because of the stronger interactions with the fixed charged groups that can form isolated ionic domains not well interconnected each other [39,42].

The density of the fixed charges of the Fuji-CEM-80050 was lower than that of the Fuji-AEM-80045 over the entire range of concentration investigated (Fig. 9B). As a consequence, this membrane was more sensitive to shrinking going from the 0.5 to the 4 M solution with respect the Fuji-AEM-800445 (-21% of mass swelling vs. -7%) because of the higher osmotic pressure difference between the solution and the membrane (osmotic pressure of the 0.5 and 4 M NaCl solutions were respectively 2.5 MPa [43] and 22 MPa [44]).

The results obtained with the Fuji-AEM-80045 and Fuji-CEM-80050 tested with the 4 M NaCl solution, did not contradict the results obtained with the Fuji-AEM-90025 and Fuji-CEM-90026 tested with the 1 M NaCl solution.

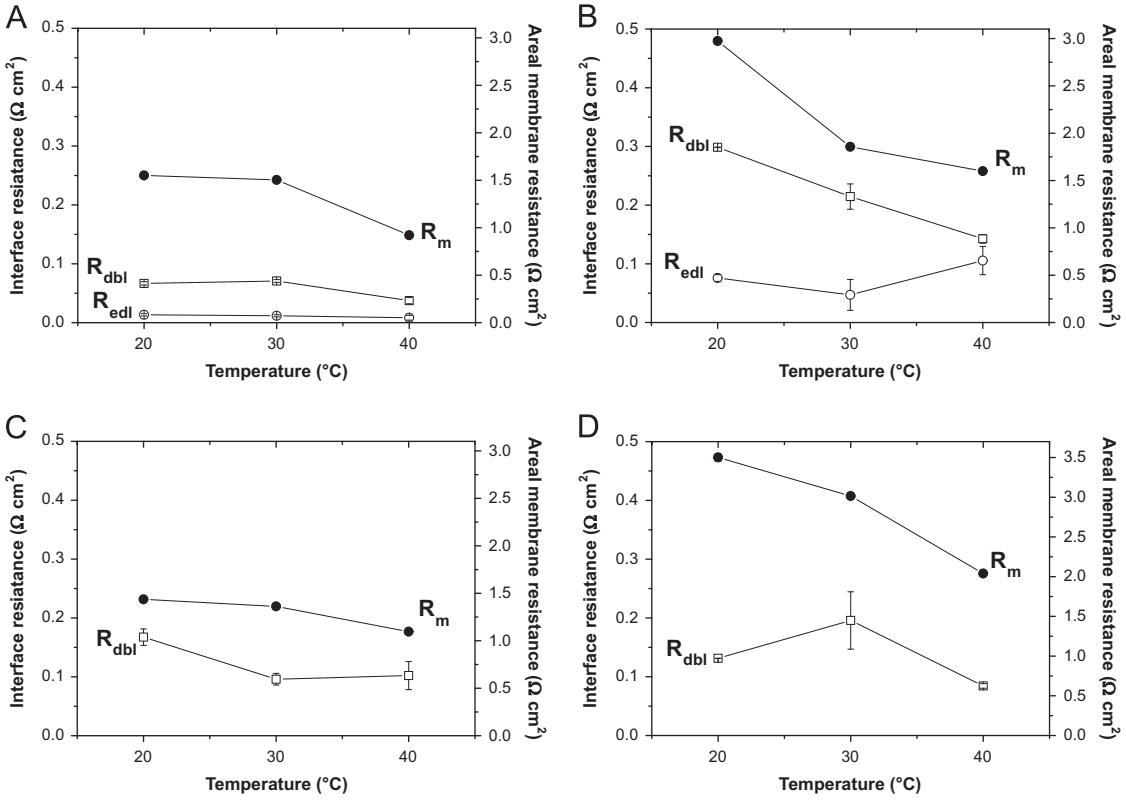

Fig. 8. Membrane (R_m) and interface (R_{edl} and R_{dbl}) areal resistances as a function of the temperature for the Fuji-AEM-80045 (A, C) and the Fuji-CEM-80050 (B, D). Conditions: 0.5 M NaCl in (A) and (B); 4 M NaCl in (C) and (D); solution velocity: 2.8 cm s^{-1}. Filled symbols, axes on the right for the R_m; empty symbols, axes on the left for the R_{edl} and R_{dbl}.

Table 2
Membrane (R_m) and interface (R_{edl} and R_{dbl}) areal resistances in NaCl solutions at various concentrations. Conditions: 2.75 cm s^{-1}, 20±1 °C.

Membrane	0.5 M			1.0 M		
	R_m (Ω cm²)	R_{edl} (Ω cm²)	R_{dbl} (Ω cm²)	R_m (Ω cm²)	R_{edl} (Ω cm²)	R_{dbl} (Ω cm²)
Fuji-AEM-90025	1.102±0.001	0.018±0.003	0.056±0.004	0.787±0.001	0.006±0.002	0.028±0.002
Fuji-CEM-90026	1.642±0.001	0.149±0.005	0.146±0.031	1.246±0.001	0.032±0.002	0.115±0.003
	0.5 M			**4.0 M**		
	R_m (Ω cm²)	R_{edl} (Ω cm²)	R_{dbl} (Ω cm²)	R_m (Ω cm²)	R_{edl} (Ω cm²)	R_{dbl} (Ω cm²)
Fuji-AEM-80045	1.551±0.001	0.013±0.002	0.067±0.003	1.436±0.001	–	0.167±0.014
Fuji-CEM-80050	2.974±0.001	0.076±0.006	0.299±0.010	3.501±0.050	–	0.131±0.001

In this second case, the membranes had an concentration of the fixed charged groups higher than the external solution (4.0 ± 0.4 for the Fuji-AEM-90025 and 2.5 ± 0.2 mol/L for the Fuji-CEM-90026 in NaCl 1 M at 20 °C), and the shrinking effect was moderate, leading to a favorable decreasing of the distance between the charged groups, but without isolating them each other. Moreover, it is well known that increasing the solution concentration the co-ion concentration in the IEM is increased, and to a first approximation is given for a monovalent salt by [45]

$$C_{co}^{m} = \frac{(C_s^s)^2}{C_{fix}} \tag{14}$$

The Eq. (14) is obtained from the Donnan equilibrium expression using the following assumptions, as described in the Ref. [45]:

the exponential function is 1, i.e.

$$e^{-(\Delta\pi \overline{V}_s / RT\nu_i z_i)} \cong 1 \tag{15}$$

the ratio of the activity coefficient in the solution and the membrane is 1, i.e.

$$\left(\frac{\gamma_{co}^{m}}{\gamma_{co}^{s}}\right)^{1/z_{co}} \left(\frac{\gamma_{cou}^{s}}{\gamma_{cou}^{m}}\right)^{1/z_{cou}} \cong 1 \tag{16}$$

and the counter ion concentration is close to the fixed ion concentration, i.e.

$$C_{cou}^{m} = C_{fix}^{m} + C_{co}^{m} \cong C_{fix}^{m} \tag{17}$$

where $\Delta\pi$ is the osmotic pressure difference between the solution and the membrane phase, C is the concentration, ν is the stoichiometric coefficient, z is the charge number, and $\overline{V}$ is the partial molar volume, the subscripts *i*, *co*, *cou*, *s* and *fix* refer to ions, co-ion, counter-ion, salt, and fixed ion of the membrane, the superscripts s and m refer respectively to membrane and solution.

Despite the obvious detrimental effect on the membrane permselectivity, the increase of the total ion concentration in

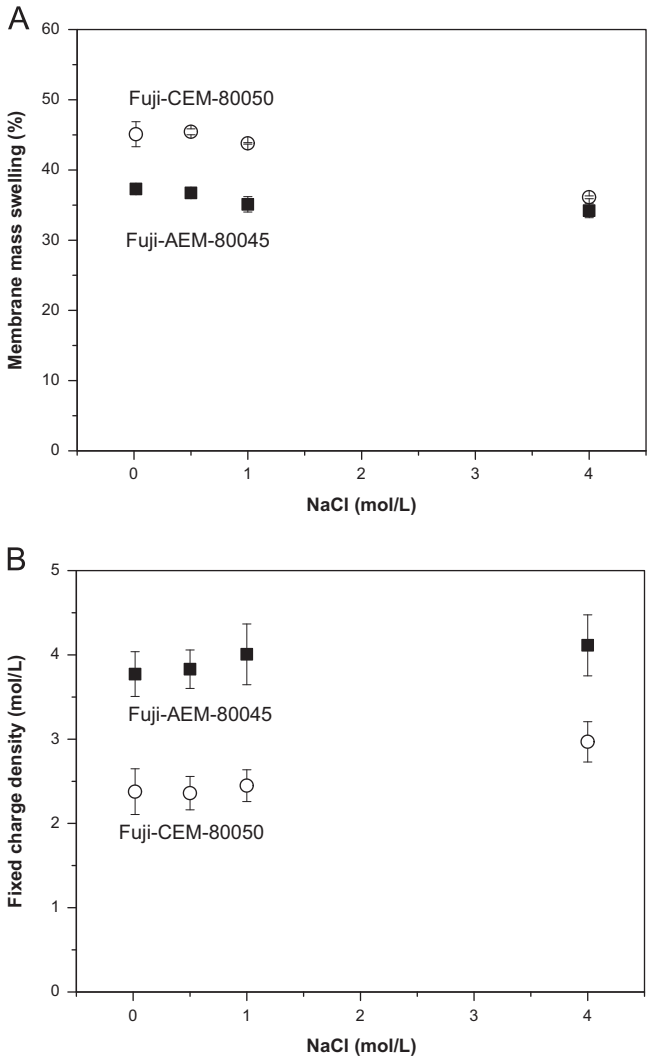

Fig. 9. Membrane mass swelling (A) and density of the fixed charges (B) of the Fuji-CEM-80050 and the Fuji-AEM-80045 as a function of the solution concentration. NaCl solution at 20 ± 1 °C.

membrane may have contributed to the reduction of the electrical resistance in the case of the test with the 1.0 M solution with respect to the test with the 0.5 M solution (higher number of current carriers).

For what concern the effect of the solution concentration on the interface resistances: increasing the concentration from 0.5 M to 1 M the resistance of both R_{edl} and R_{dbl} decreased.

However, increasing the external solution concentration from 0.5 to 4 M, the R_{dbl} increased while the R_m decreased in the case of the Fuji-AEM-80050, and the R_{dbl} decreased while the R_m increased, in the case of the Fuji-CEM-80045.

3.3. Diffusive behavior at zero solution velocity

A separate discussion of the impedance data measured at zero velocity is necessary. A peculiar feature of the spectrum registered at low frequency (< 0.1 Hz) was observed in the case of the 0.5 and 1.0 M NaCl solution, attributable to a diffusion control in the ion transport at the interface [46–49]. This phenomenon was due to the intensification of the bipolar polarization phenomena at the membrane/solution interface when the solution velocity was zero. The rising of the polarization phenomena was due to the absence of turbulences induced by the solution recirculation. The appearance of the diffusive component was reversible and it can be eliminated by restarting the solution recirculation. Various increasing and decreasing velocity runs were performed to confirm this point.

The Nyquist plot registered at frequency < 0.1 Hz with the membrane in 0.5 M solution, had an angle of about 45° (Fig. 10A and B). Moreover, plotting the absolute value of the real and imaginary part of the impedance (|Z'| and |Z″|) vs. $1/\sqrt{2\pi\upsilon}$ two straight and parallel lines were obtained and the slope of both lines was equal to the coefficient of the Warburg impedance σ [$\Omega\,s^{-1/2}$] [47–52]. Also with the 1.0 M solution a diffusive behavior can be observed in the Nyquist plot (Fig. 10C). In the case of the 4 M NaCl solution, the diffusive behavior was not visible in the impedance spectra because of the reducing of the thickness (and resistance) of the electrical double layer with the concentration (Fig. 10D).

The counter-ion diffusion coefficient (D_{ion} [$cm^2\,s^{-1}$]) was calculated according to the following equation [47–52]:

$$D_{ion} = \left(\frac{RT}{\sqrt{2}AF^2\sigma C_{fix}}\right)^2 \tag{18}$$

where R is the gas constant [8314 J K^{-1} mol^{-1}], T the temperature [K], A the membrane area [cm^2], F Faraday's constant [96485 A s mol^{-1}], σ the coefficient of Warburg impedance [$\Omega\,s^{-1/2}$] and C_{fix} is the concentration of the fixed charged groups in membrane [expressed as mol cm^{-3}].

The σ coefficient was obtained by fitting the impedance spectrum with the equivalent circuit showed in Fig. 2C. Despite in literature the Warburg impedance has been usually related to diffusion phenomena in DBL [51–54], in our opinion, the diffusive behavior is also related to phenomena occurring in the DL of the EDL. This hypothesis was formulated on the basis of the disappearance of the diffusive behavior testing the membranes in 4 M solution, e.g. in conditions in which the contribution of the EDL become negligible.

The Nova software returned the parameter Y^o [$S\,s^{½}$] which is related to the Warburg coefficient by the following relationship:

$$\sigma = \frac{1}{\sqrt{2}Y^o} \tag{19}$$

The calculated diffusion coefficient for the AEMs and CEMs depended from the reciprocal of the square of the density of the fixed charged groups in membrane (Eq. (15)). The bipolar polarization phenomena are expected to increase increasing the density of the fixed charged groups because of the higher attraction of the membrane for the counter ions. Moreover, increasing the fixed charge density the counter ions are "less free" to diffuse and the diffusion coefficient decreases. As a consequence, ion diffusion coefficient in a not ideal system, cannot be considered as an intrinsic parameter of the ion, and the effect of the chemical micro-environment cannot be overlooked. As a consequence the observed order in the ion diffusion coefficient for the AEMs was Fuji-AEM-0150 > Fuji-AEM-90025 > Fuji-AEM-80045 (Table 3). For the same reason, the order for the CEMs was Fuji-CEM-90026 > Fuji-CEM-80050 > Fuji-CEM-0150.

Also the increasing of the membrane electrical resistance favored bipolar polarization, because of the slower ion transport in membrane. This was the reason of the jump of the diffusion coefficient of the Fuji-CEM-90026 with respect to the other two CEMs (Table 3), because this sample had a significantly lower membrane electrical resistance, combined also with a lower density of the fixed charged groups. A third factor able to influence ion diffusivity is the ion mobility. The AEMs had a higher diffusion coefficient than the CEMs, and the values increased with the

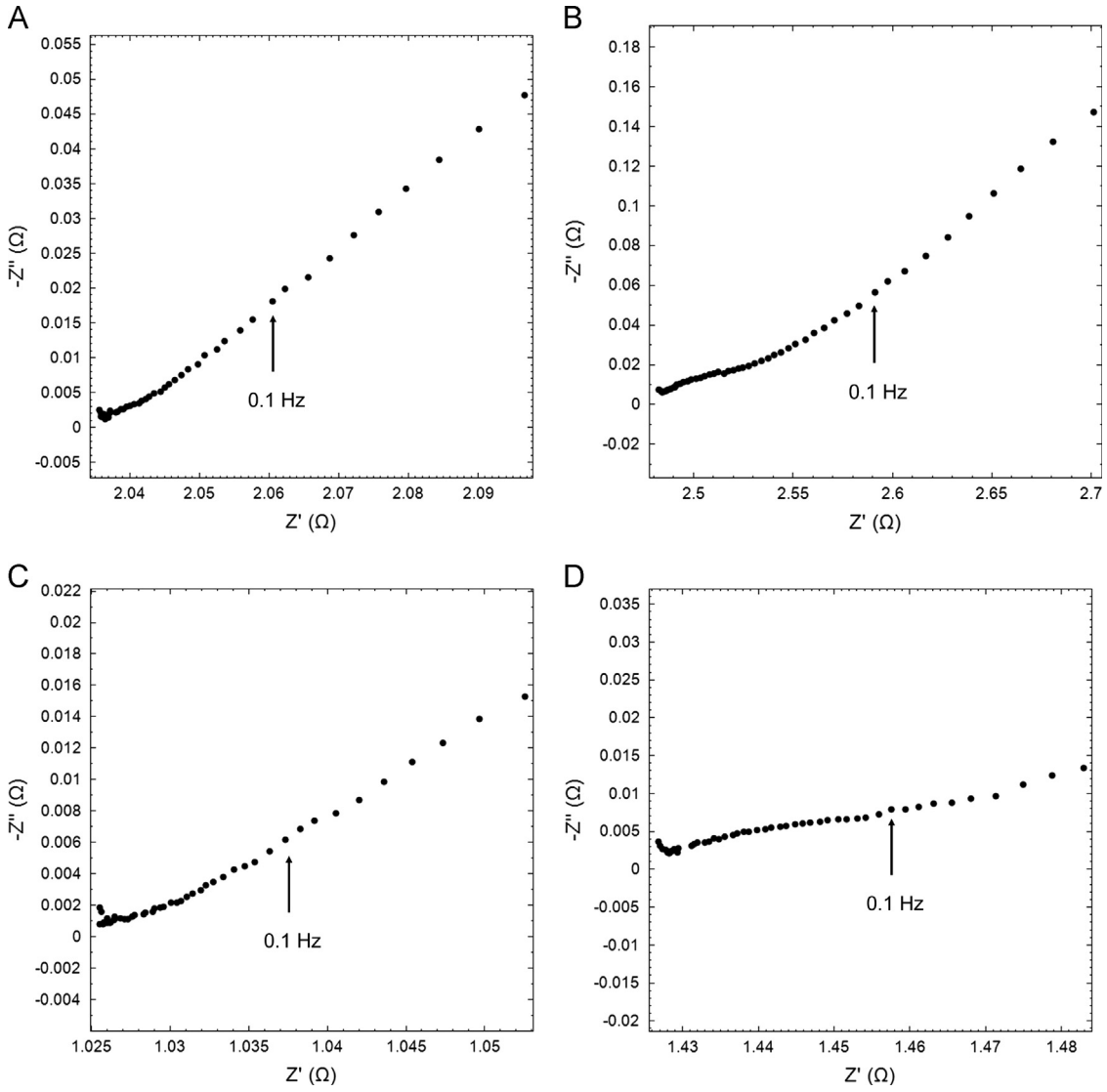

Fig. 10. Nyquist plot of the Fuji-AEM-80045 and the Fuji-CEM-80050 membranes measured in a 0.5 M (A and B respectively), Fuji-AEM-90025 in 1.0 M NaCl and Fuji-CEM-80050 in a 4.0 M NaCl solution (D) at zero solution velocity and 20 ± 1 °C.

Table 3
Ion diffusion coefficient obtained from impedance data registered at zero solution velocity

Membrane	Diffusion coefficient ($cm^2\ s^{-1}$) of Na^+ (for CEMs) and Cl^- (for AEMs)			
	@ 20 °C; 0.5 M NaCl	@ 30 °C (corr sw); 0.5 M NaCl	@ 40 °C (corr sw); 0.5 M NaCl	@ 20 °C; 1 M NaCl
Fuji-AEM-0150	4.61×10^{-6}	–	–	–
Fuji-AEM-80045	1.46×10^{-6}	1.60×10^{-6}	1.81×10^{-6}	
Fuji-AEM-90025	3.52×10^{-6}	–	–	1.74×10^{-5}
Fuji-CEM-0150	2.15×10^{-7}	–	–	–
Fuji-CEM-80050	3.83×10^{-7}	4.26×10^{-7}	6.89×10^{-7}	–
Fuji-CEM-90026	9.48×10^{-7}	–	–	4.57×10^{-6}

temperature. For what concern the effect of the solution concentration, increasing the concentration from 0.5 to 1 M, an increase in the diffusion coefficient was observed because of the increasing screening effect of the attractive electrical interactions between the counter-ions in the DL and fixed charged groups of the membrane. The ions in the DL are less attracted to the charged membrane surface and they tend to diffuse (back-diffuse) into the bulk phase under the influence of electrical attraction and thermal motion.

3.4. NMR investigation

The temperature evolution of the ^1H NMR spectra, collected from 20 °C up 100 °C on the Fuji-AEM-80045 and Fuji-CEM-80050

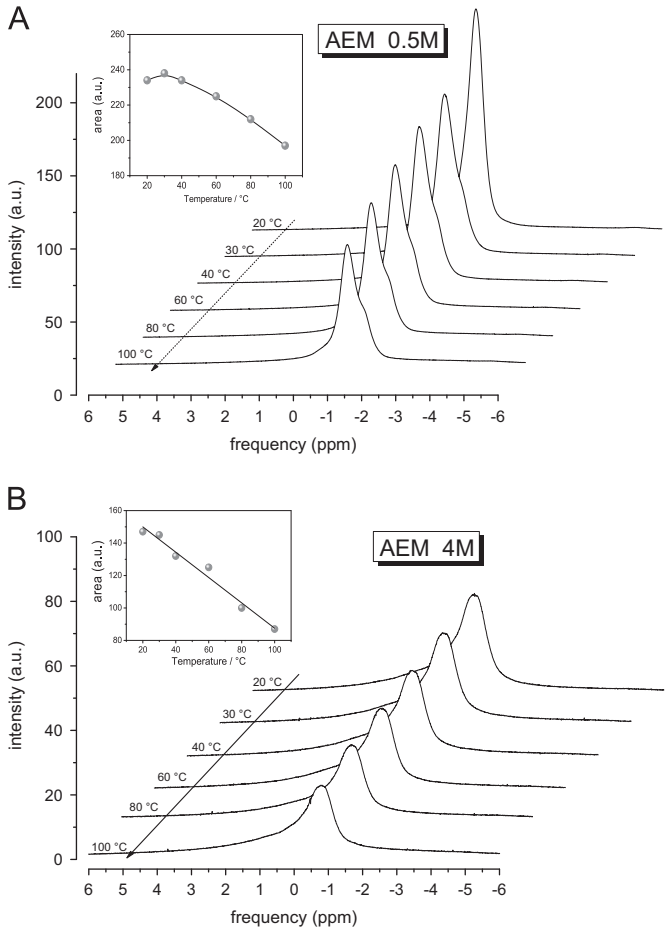

Fig. 11. Temperature evolution of ^{1}H–NMR spectra collected on the Fuji-AEM-80045 membranes swelled in water salt solution at two concentrations, 0.5 and 4 M. The inset shown the peak area vs. temperature.

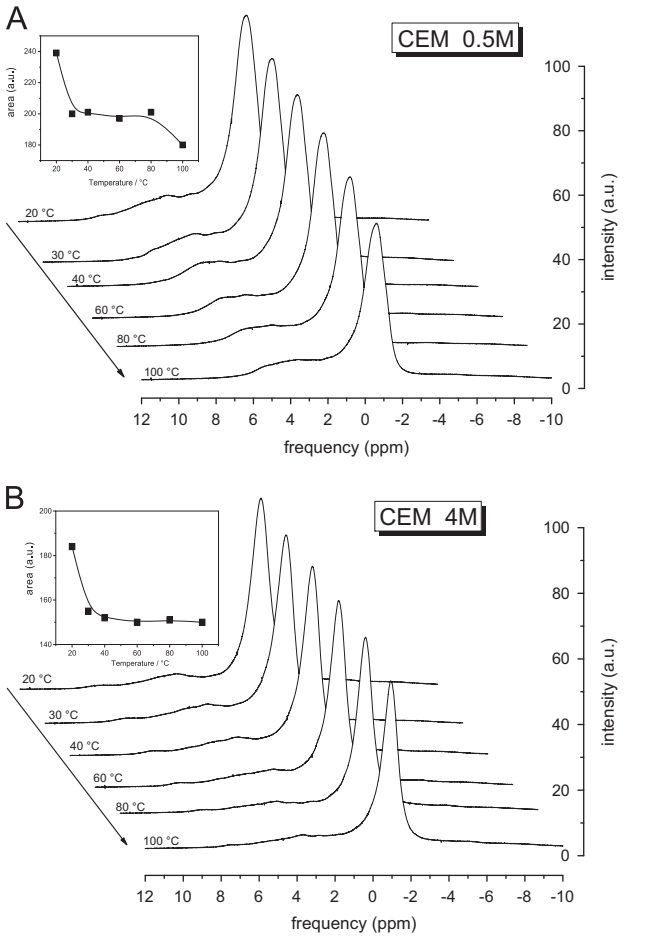

Fig. 12. Temperature evolution of ^{1}H–NMR spectra collected on the Fuji-CEM-80050 membranes swelled in water salt solution at two concentrations, 0.5 and 4 M. The inset shown the peak area vs. temperature.

membranes, swelled in 0.5 and 4 M NaCl solutions, are reported respectively in Figs. 11 and 12, respectively. All the spectra were acquired with the same number of scans ($ns=4$) and were referenced against pure water set at 0 ppm. The NMR signal essentially originates from the water of the salt solutions absorbed from the membranes, while, the proton signals of the polymer chains are basically "invisible", both because their intensity is very small compared to the signal intensity of the water, and because the dipolar spin-spin interactions make hugely broaden the spectral lines.

The proton's signal of both Fuji-AEM-80045 and Fuji-CEM-80050, was quite large (FWHM was about 1 kHz) and asymmetric, typical of a multiple components configuration, i.e., different "types" of water coexist in the system. Actually, water was involved in the hydration shells of the fixed ionic groups of the polymer matrix, as well as, of the mobile ions. However, the different states of water within the hydrophilic channels can be difficult to be discerned because of the fast rate of exchange and, for this reason, only one peak was seen. The intensity of this peak decreased with increasing temperature because of the water evaporation from the membrane (inset in Figs. 11 and 12 shown the peak area vs. temperature).

For the Fuji-AEM-80045 the proton signal of the membrane swelled with the 0.5 M solution was more intense and narrow than membrane swelled in 4 M (Fig. 11). This was due to the higher solution uptakes and to the greater amount of bulk/"free" water (water molecules not involved in the hydration shells of the ions), respectively. The bulk/"free" water originates a narrower Lorentzian signal and, by heating, it was reasonable to expect that this evaporates before, while the "bound" water was more retained in the membrane pores and the strong interactions cause a broadening of the NMR signal.

For the Fuji-CEM-80050, the spectral line for the two concentrations, was very similar and different from that observed in the anionic membrane (Fig. 12). Indeed, in the Fuji-CEM-80050 was present a peak quite Lorentzian accompanied by a broad shoulder in the region of higher frequency. The shape of the spectral line of water confined in membrane clearly depends on the structural and morphological nature of the membrane itself, such as hydrophilic channels size and ionic functional groups present within them, as well as by the nature (size and charge) of the solvated ions. In the CEM, the hydration of the Na^{+} cations involves a greater number of water molecules (hydration number is 5 ± 1), i.e. sodium ion has a greater hydrodynamic radius, than that of the Cl^{-} anions (hydration number is 1 ± 1). Furthermore, the different orientation of water molecules (H pointed toward anions and oxygen toward cations), which arises from the charge asymmetry of the water molecule, results in an effect on the chemical shift of water protons, as was clear from the spectra. The Fuji-CEM-80050 swelled in 0.5 M solution showed a more pronounced shoulder signal than the 4 M, probably imputable to the greater number of water molecules bounded to the ionic groups in the hydrophilic channels. Instead, the decrease of the total area of

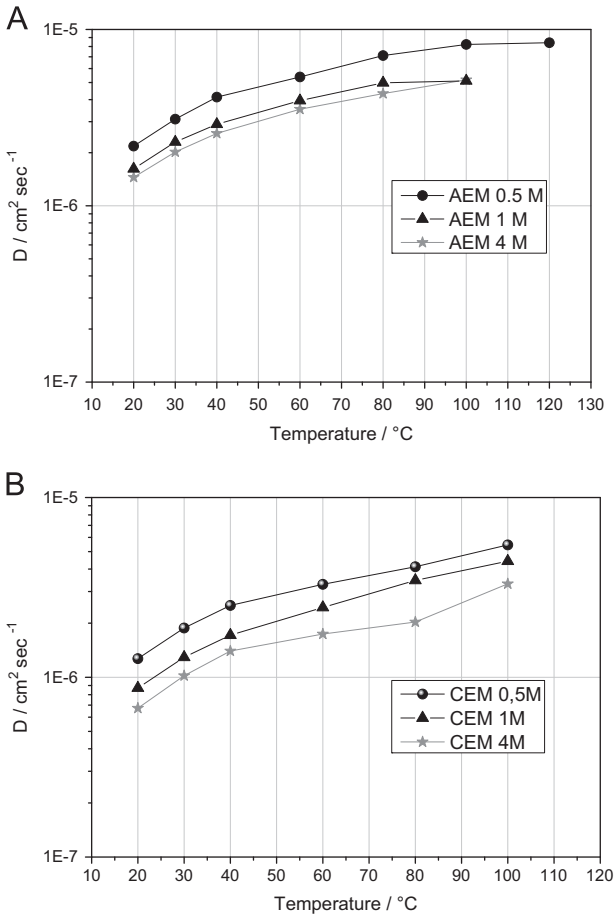

Fig. 13. Self-diffusion coefficients of water confined in completely swelled membranes, from 20 °C up to 100 °C. AEM indicates the Fuji-AEM-80045; CEM indicates the Fuji-CEM-80050.

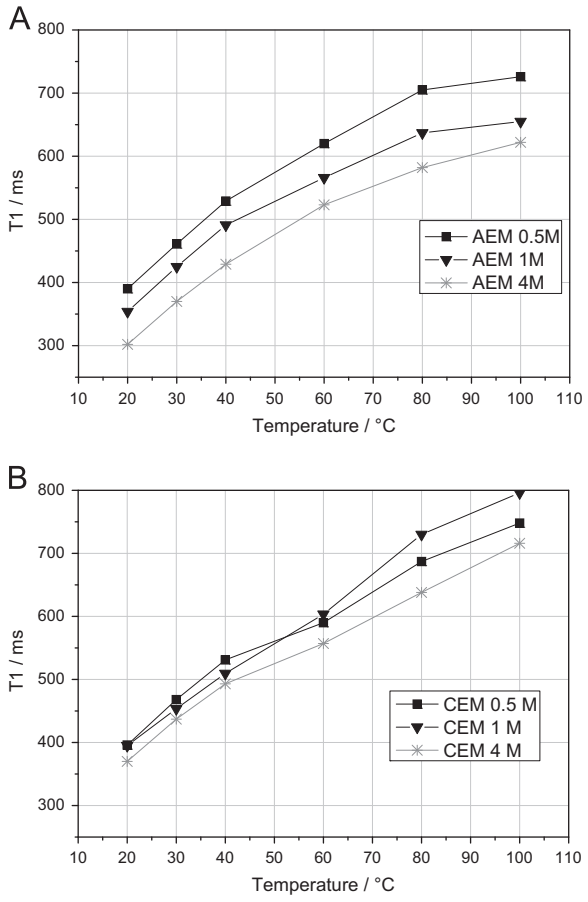

Fig. 14. Longitudinal relaxation times T1 as a function of the temperature (from 20 to 140 °C) of the water confined in completely swelled membranes. AEM indicates the Fuji-AEM-80045; CEM indicates the Fuji-CEM-80050.

the signal in temperature follows the same trend for both concentrations.

The self-diffusion coefficients (D) of water confined in the Fuji-AEM-80045 and Fuji-CEM-80050 swelled up to saturation in salt solutions at three different concentrations, 0.5 M, 1 M and 4 M, are reported in Fig. 13 as a function of temperature, from 20 °C up to 100 °C.

It is well established that when solvent molecules (water in this case) diffuse in presence of macromolecules, their diffusion is slowed down by both the need to divert around macromolecules (obstruction effect) and any interactions with the same macromolecules that inhibit their motion [55,56]

The latter effect, i.e. the interaction between solvent and macromolecules, may be termed solvation or hydration and we can affirm that the interacting molecules are in the "bound state". Exchange of molecules between bound- and free-state results in an averaged water diffusion coefficient D, which depends on the time fraction spent in each state. Additionally, in this case a salt solutions was present, so, water molecules are also involved in the hydration of sodium and chlorine ions and their transport by a vehicular mechanism.

From the data emerged that the ions mobility decreased with increasing the solution concentration while, overall, in the Fuji-CEM-80050, the water diffusion was lower than in the Fuji-AEM-80045.

The decreasing of D when the concentration of the solution increases was due to:

(i) the greater amount of ions that entails a greater number of hydration water molecules, then less mobile;

(ii) the reduction of hydrophilic channels size, that was correlated to the swelling/shrinking of the membrane and that brings a higher obstruction effect and at a reduction of the amount of "free" water.

Finally, as expected, the water diffusion in the AEM was higher than in CEM, since in the AEM, chlorine ions have a number of hydration much smaller than that of the sodium ion in the CEM, therefore, more "free" water in the first membrane and less in the second, at the same concentration.

Further information on the molecular dynamic of the molecules was provided by measurements of longitudinal (or spin-lattice) relaxation times (T_1), as reported in Fig. 14.

Compared to diffusion, T_1 reflects more localized motions including both translation and rotation on a time scale comparable to the reciprocal of the NMR angular frequency ($\sim$1 ns). As the molecular correlation time τ_c depends on temperature, a minimum in T_1 is often observed when $\overline{\omega}\tau_c \sim 1$, where $\overline{\omega}$ is the NMR frequency [57].

In the temperature range investigated, well above the T_1 minimum, i.e. in the so-called extreme narrowing limit ($\overline{\omega}\tau_c \ll 1$), higher T_1 values suggest more facile molecular rotational and translational motion.

In both two membranes, the T_1 values fall into the same range, between 300 and 800 ms, with an almost linear increase with the temperature. Respect to D, T_1 is less affected from the hydrophilic channels size, while the ionic interactions and the molecular aggregations are important. In fact, the solution concentration in the anionic membrane shows a well marked effect, less defined in

the cationic membrane. This could be attributed to the different ionic hydration (orientation of the water molecules in the hydration sphere, and hydration number).

4. Conclusions

The Electrochemical Impedance Spectroscopy is a powerful, non-invasive and non-destructive, technique to characterize the ion transport resistance through membranes and interfacial layers formed when an ion exchange membrane is in contact with an electrolyte solutions (electrical double layer and diffusion boundary layer). The cation exchange membranes were characterized by an higher electrical resistance in comparison with the anion exchange membranes in NaCl solutions. This behavior was explained considering the higher mobility of the Cl^- with respect to the Na^+ (the counter ions of the ion exchange membranes).

The areal membrane resistance was the dominant resistance in the whole range of solution concentration, temperature and velocity investigated (0.5–4.0 M; 20–40 °C; 0–4.0 cm s^{-1}) and it did not depend significantly from the velocity. On the contrary, the resistance of the diffusion boundary layer was reduced increasing the solution velocity.

A diffusive component in the ion transfer at the interface membrane/solution was evident operating in static conditions (zero velocity, no solution stirring), at concentrations $\leq$ 1.0 M.

It was demonstrated that increasing the solution concentration the resistance of the double electrical layer was reduced, and it became negligible at 4 M. This effect was due to the increasing screening of the attractive electrical interactions between the counter-ions and fixed charged groups of the membrane, increasing the concentration of the external solution.

Increasing the solution concentration from 0.5 to 4.0 M the membrane resistance decreases for the Fuji-AEM-80045 but increased for the Fuji-CEM-80050. An opposite behavior was observed for the resistance of the diffusion boundary layer. The increased electrical resistance in 4.0 M solution of the Fuji-CEM-80050 membrane was due to its low fixed charge density in comparison with the external solution, which induced an high osmotic pressure difference between the solution and the membrane phase, and the consequent membrane shrinking and narrowing of the hydrophilic channels pathway for the ions transport. As a consequence it was evident the importance to use membranes with a fixed charge density higher than the solution in the case of concentrated electrolyte solutions.

The relevant effect of the solution concentration on the membrane microstructure was confirmed by pulsed gradient spin echo (PGSE)-NMR technique. From the data clearly emerged that the water self diffusion coefficient decreased with increasing the solution concentration. In parallel the strong increase of fixed charged groups density, increased the resistance to the ion migration.

Acknowledgments

This work was partially funded in the framework of the REAPower project (Reverse Electrodialysis Alternative Power production) (www.reapower.eu), EU-FP7 programme (Project no. 256736).

References

[1] E. Barsoukov, J.R. Macdonald, Impedance Spectroscopy. Theory, Experiment, and Applications, Second Edition, John Wiley & Sons, New Jersey, 2005.
[2] N. Islam, N.A. Bulla, S. Islam, Electrical double layer at the peritoneal membrane/electrolyte interface, J. Membr. Sci. 282 (2006) 89–95.
[3] S. Sang, Q. Wu, K. Huang, A discussion on ion conductivity at cation exchange membrane/solution interface, Colloids Surf., A 320 (2008) 43–48.
[4] H. Strathmann, Ion-Exchange Membrane Separation, Elsevier, Amsterdam, 2004.
[5] H.G.L. Coster, T.C. Chilcott, A.C.F. Coster, Impedance spectroscopy of interfaces, membranes and ultrastructures, Bioelectrochem. Bioenergy 40 (1996) 78–96.
[6] T.C. Chilcott, M. Chna, L. Gaedt, T. Nantawisarakul, A.G. Fane, H.G.L. Coster, Electrical impedance spectroscopy characterization of conducting membranes, J. Membr. Sci. 195 (2002) 153–167.
[7] X. Dominguez-Benetton, S. Sevda, K. Vanbroekhoven, D. Pant, The accurate use of impedance analyses for the study of microbial electrochemical systems, Chem. Soc. Rev. 41 (2012) 7228–7246.
[8] G. Alberti, M. Casciola, L. Massinelli, B. Bauer, Polymeric proton conducting membranes for medium temperature fuel cells (110–160 °C), J. Membr. Sci. 185 (2001) 73–81.
[9] K.-V. Peinemann, S. Pereira Nunes, Membranes for Energy Conversion, Wiley–VCH, Chichester, 2008.
[10] E. Fontananova, F. Trotta, J.C. Jansen, E. Drioli, Preparation and characterization of new non-fluorinated polymeric and composite membranes for PEMFCs, J. Membr. Sci. 348 (2010) 326–336.
[11] E. Fontananova, V. Cucunato, E. Curcio, F. Trotta, M. Biasizzo, E. Drioli, G. Barbieri, Influence of the preparation conditions on the properties of polymeric and hybrid cation exchange membranes, Electrochim. Acta 66 (2012) 164–172.
[12] W. Zhang, U.E. Spichiger, An impedance study on Mg^{2+} selective membrane, Electrochim. Acta 45 (2000) 2259–2266.
[13] J. Benavente, A. Canas, M.J. Ariza, A.E. Lozano, J. de Abajo, Electrochemical parameters of sulfonated poly(ether ether sulfone) membranes in HCl solutions determined by impedance spectroscopy and membrane potential measurements, Solid State Ionics 145 (2001) 53–60.
[14] F. Treptowa, A. Jungbauerb, K. Hellgardta, Halide diffusion in polyaniline membranes, J. Membr. Sci. 270 (2006) 115–122.
[15] J. O'M. Bockris, F.B. Diniz, Aspects of electron transfer at a conducting membrane–solution interface, Electrochim. Acta 34 (1989) 561–575.
[16] J.S. Park, T.C. Chilcott, H.G.L. Coster, S.H. Moon, Characterization of BSA-fouling of ion-exchange membrane systems using a subtraction technique for lumped data, J. Membr. Sci. 246 (2005) 137–144.
[17] A. Antony, T. Chilcott, H. Coster, G. Leslie, In situ structural and functional characterization of reverse osmosis membranes using impedance spectroscopy, J. Membr. Sci. 425–426 (2013) 89–97.
[18] J.-S. Park, J.-H. Choi, J.-J. Woo, S.-H. Moon, An electrical impedance spectroscopic (EIS) study on transport characteristics of ion-exchange membrane systems, J. Colloid Interface Sci. 300 (2006) 655–662.
[19] P. Długołecki, P. Ogonowski, S.J. Metz, M. Saakes, K. Nijmeijer, M. Wessling, On the resistances of membrane, diffusion boundary layer and double layer in ion exchange membrane transport, J. Membr. Sci. 349 (2010) 369–379.
[20] Y. Xu, M. Wang, Z. Ma, C. Gao, Electrochemical impedance spectroscopy analysis of sulfonated polyethersulfone nanofiltration membrane, Desalination 271 (2011) 29–33.
[21] Yaoming Wang, Anlei Wang, Xu Zhang, Tongwen Xu, The concentration, resistance, and potential distribution across a cation exchange membrane in 1:2 (Na_2SO_4) type aqueous solution, Desalination 284 (2012) 106–115.
[22] J.M. Kavanagh, S. Hussain, T.C. Chilcott, H.G.L. Coster, Fouling of reverse osmosis membranes using electrical impedance spectroscopy: measurements and simulations, Desalination 236 (2009) 187–193.
[23] Y. Gao, W. Li, W.C.L. Lay, H.G.L. Coster, A.G. Fane, C.Y. Tang, Characterization of forward osmosis membranes by electrochemical impedance spectroscopy, Desalination 312 (2013) 45–51.
[24] J. Cen, J. Kavanagh, H. Coster, G. Barton, Fouling of reverse osmosis membranes by cane molasses fermentation wastewater: detection by electrical impedance spectroscopy techniques, Desalin. Water Treat. 51 (4–6) (2013) 969–975.
[25] T. Lopes, L. Andrade, H.A. Ribeiro, A. Mendes, Characterization of photoelectrochemical cells for water splitting by electrochemical impedance spectroscopy, Int. J. Hydrogen Energy 35 (2010) 11601–11608.
[26] B.E. Logan, M. Elimelech, Membrane-based processes for sustainable power generation using water, Nature 488 (7411) (2012) 313–319and references therein 488 (7411) (2012).
[27] K.P. Lee, T.C. Arnot, D. Mattia, A review of reverse osmosis membrane materials for desalination—development to date and future potential, J. Membr. Sci. 370 (2011) 1–22.
[28] D. Winter, J. Koschikowski, M. Wieghaus, Desalination using membrane distillation: experimental studies on full scale spiral wound modules, J. Membr. Sci. 375 (2011) 104–112.
[29] X. Ji, E. Curcio, S. Al Obaidani, G. Di Profio, E. Fontananova, Enrico Drioli, Membrane distillation–crystallization of seawater reverse osmosis brines, Sep. Purif. Technol. 71 (2010) 76–82.
[30] M. Tedesco, A. Cipollina, A. Tamburini, W. van Baak, G. Micale, Desalin. Water Treat. 49 (2012) 404–424.
[31] E. Brauns, Salinity gradient by reverse electrodialysis: effect of model parameters on electrical power output, Desalination 237 (2009) 378–391.
[32] E. Brauns, Finite elements-based 2D theoretical analysis of the effect of IEX membrane thickness and salt solution residence time on the ion transport within a salinity gradient power reverse electrodialysis half cell pair, Desalin. Water Treat. (2013) 1–15.
[33] E.O. Stejskal, J.E. Tanner Spin, Diffusion measurements: spin echoes in the presence of a time-dependent field gradient, J. Chem. Phys. 42 (1965) 288–292.
[34] R.J. Hunter, Zeta Potential in Colloid Science, Academic Press, London, 1981.

[35] J.A. Manzanares, W.D. Murpby, S. Maffè, H. Reiss, Numerical simulation of the nonequilibrium diffuse double layer in ion-exchange membranes, J. Phys. Chem. 97 (1993) 8524–8530.
[36] C. Larchet, S. Nouri, B. Auclair, L. Dammak, V. Nikonenko, Application of chronopotentiometry to determine the thickness of diffusion layer adjacent to an ion-exchange membrane under natural convection, Adv. Colloid Interface Sci. 139 (2008) 45–61.
[37] A.A. Moya, P. Sistat, Chronoamperometric response of ion-exchange membrane systems, J. Membr. Sci. 444 (2013) 412–419.
[38] S. Koneshan, J.C. Rasaiah, R.M. Lynden-Bell, S.H. Lee, Solvent structure, dynamics, and ion mobility in aqueous solutions at 25 °C, J. Phys. Chem. B 102 (1998) 4193–4204.
[39] K.A. Mauritz, R.B. Moore, State of understanding of nafion, Chem. Rev. 104 (2004) 4535–4558.
[40] K. Bohinc, V. Kralj-Iglic, A. Iglic, Thickness of electrical double layer. Effect of ion size, Electrochim. Acta 46 (2001) 3033–3040.
[41] W.B. Russel, D.A. Saville, W.R. Schowalter, Colloidal Dispersions, Cambridge University Press, Cambridge, 1989.
[42] K.D. Kreuer, On the development of proton conducting polymer membranes for hydrogen and methanol fuel cells, J. Membr. Sci. 185 (2001) 29–39.
[43] J.R. McCutcheon, R.L. McGinnis, M. Elimelech, Desalination by ammonia–carbon dioxide forward osmosis: influence of draw and feed solution concentrations on process performance, J. Membr. Sci. 278 (2006) 114–123.
[44] Y. Luo, B. Roux, Simulation of osmotic pressure in concentrated aqueous salt solutions, J. Phys. Chem. Lett. 1 (2010) 183–189.
[45] H. Strathmann, Electromembrane processes: basic aspects and application, in: Enrico Drioli, Lidietta Giorno (Eds.), Comprehensive Membrane Science and Engineering, vol. 2, Elsevier, Oxford, 2010, pp. 391–429.
[46] R.D. Armstrong, J.C. Lockhart, M. Todd, The mechanism of transfer of K^+ between aqueous solution and PVC membranes containing valinomycin, Electrochim Acta 31 (1986) 591–594.
[47] P.P. Prosini, M. Lisi, D. Zane, M. Pasquali, Determination of the chemical diffusion coefficient of lithium in $LiFePO_4$, Solid State Ionics 148 (2002) 45–51.
[48] A.A. Moya, Electric circuits modelling the low-frequency impedance of ideal ion-exchange membrane systems, Electrochim. Acta 62 (2012) 296–304.
[49] P. Sistat, A. Kozmai, N. Pismenskaya, C. Larchet, G. Pourcelly, V. Nikonenko, Low-frequency impedance of an ion-exchange membrane system, Electrochim. Acta 53 (2008) 6380–6390.
[50] Donald R. Franceschetti, J. Ross Macdonald, Richard P. Buck, Interpretation of finite-length-Warburg-type impedances in supported and unsupported electrochemical cells with kinetically reversible electrodes, J. Electrochem. Soc. 138 (1991) 1368–1371.
[51] N. Fouquet, C. Doulet, C. Nouillant, G. Dauphin-Tanguy, B. Ould-Bouamam, Model based PEM fuel cell state-of-health monitoring via ac impedance measurements, J. Power Sources 159 (2006) 905–913.
[52] S.A. Mareev, V.V. Nikonenko, A numerical experiment approach to modeling impedance: application to study a Warburg-type spectrum in a membrane system with diffusion coefficients depending on concentration, Electrochim. Acta 81 (2012) 268–274.
[53] M. Shi, Z. Chen, J. Sun, Determination of chloride diffusivity in concrete by AC impedance spectroscopy, Cement Concr. Res. 29 (1999) 1111–1115.
[54] F. Treptow, A. Jungbauer, K. Hellgardt, Halide diffusion in polyaniline membranes, J. Membr. Sci. 270 (2006) 115–122.
[55] L. Coppola, R. Muzzalupo, G.A. Ranieri, Temperature dependence of water self-diffusion in the gel phase of a potassium palmitate system, J. Phys. II 6 (1996) 657–666.
[56] A. Gottwald, L.K. Creamer, P.L. Hubbard, P.T. Callaghan, Diffusion, relaxation and chemical exchange in casein gels: a nuclear magnetic resonance study, J. Chem. Phys. 122 (2005) 34506–34515.
[57] C.P. Slichter, Principles of Magnetic Resonance, 3rd ed. Springer ed., Springer Series in Solid State Science, New York, 1990.